A novel CEST-based approach for reliably assessing skeletal muscle oxidative phosphorylation: OXCEST

Ritambhar Burman,[1] Yuxi Pang,[1] Asim Bag,[1] Richard Finkel,[2] Kirsten Ness,[3] Puneet Bagga[1]

Affiliations

[1]Department of Radiology, St. Jude Children's Research Hospital, Memphis, TN, USA

[2]Department of Pediatric Medicine, St. Jude Children's Research Hospital, Memphis, TN, USA

[3]Department of Epidemiology and Cancer Control, St. Jude Children's Research Hospital, Memphis, TN, USA

Word Count: 4495

Corresponding Author:

Puneet Bagga, PhD

Department of Radiology

St. Jude Children's Research Hospital

262 Danny Thomas Place, MS 220

Memphis, TN, 38105-3678 USA

Email: puneet.bagga@stjude.org

Abstract

Purpose: To develop and validate a novel chemical exchange saturation transfer (CEST) MRI method to map skeletal muscle OXPHOS (Oxidative Phosphorylation CEST or OXCEST).

Theory and Methods: Our proposed OXCEST method acquires creatine (Cr)-weighted CEST maps by applying RF saturation (B_1) at only two frequency offsets: +1.8 ppm (targeting the Cr amine resonance) and -1.8 ppm (to calculate MTR_{asym} at 1.8 ppm). The pre-exercise MTR_{asym} is modeled as a second-order polynomial function (f) of B_0. Next, the post-exercise alteration in MTR_{asym} is hypothesized to be affected by both an exercise-induced increase in Cr and changes in B_0 inhomogeneity. By inputting post-exercise B_0 values into f, the change in MTR_{asym} due to B_0 variation alone was estimated. Thus, the Cr-related post-exercise MTR_{asym} could be isolated and quantified. OXCEST and 31P-MRS were performed in seven subjects across two sessions to compare the OXCEST-derived Cr recovery time constant (T_{Cr}) with the ground-truth phosphocreatine recovery time constant (T_{PCr}).

Results: A second-order polynomial function f could reliably describe the relationship between pre-exercise MTR_{asym} and B_0 (R^2=0.87±0.07 in the lateral gastrocnemius (LG); R^2=0.98±0.01 in the medial gastrocnemius (MG); R^2=0.96±0.03 in the soleus). The mean pre-exercise MTR_{asym} was approximately 6-7% for all muscle groups. Following exercise, MTR_{asym} increased by 11.4±4.5% in LG and 8±2.4% in MG, and showed mono-exponential recovery (R^2>0.97). The combined T_{Cr} of LG and MG was found to be significantly correlated with T_{PCr} (R^2=0.83, p=0.005).

Conclusion: OXCEST enables reliable assessment of post-exercise Cr recovery and demonstrated strong agreement with 31P-MRS.

Keywords: CEST, Cr, PCr, skeletal muscle, OXPHOS

1 | INTRODUCTION

Mitochondrial oxidative phosphorylation (OXPHOS) is a critical metabolic pathway that produces adenosine triphosphate (ATP), the primary energy currency. OXPHOS capacity varies significantly across populations, with endurance athletes exhibiting considerably greater mitochondrial activity compared to sedentary lean or overweight individuals.[1] Conversely, compromised mitochondrial OXPHOS is associated with various pathological conditions including neuromuscular disorders, mitochondrial diseases, and aging.[2-5] Currently, invasive muscle biopsy represents the gold-standard method to assess OXPHOS capacity.[6] However, biopsies have inherent limitations, including patient discomfort, risk of complications, and limited feasibility for repeated assessments over time. 31-Phosphorus magnetic resonance spectroscopy (31P-MRS) has traditionally been regarded as the MR-based gold standard technique to non-invasively quantify mitochondrial function in skeletal muscle.[7-11] Phosphocreatine (PCr) is hydrolyzed during muscle contraction to regenerate ATP from ADP, and subsequently resynthesized during recovery phase through the creatine kinase (CK) reaction, which biochemically couples PCr and creatine (Cr).[12,13] 31P-MRS has been increasingly used to investigate mitochondrial dysfunction in aging and mitochondrial disorders.[8,14-16] However, the broader application of 31P-MRS is challenged by its relatively low intrinsic sensitivity, the need for specialized hardware, and lower spatial resolution compared to proton-based imaging techniques.

To address this, the foundation for proton imaging of Cr was established by Haris et al.,[17] who identified sharp amine proton resonances of Cr at +1.8 ppm. Kogan et al.[18,19] subsequently demonstrated that chemical exchange saturation transfer (CEST) imaging could map Cr in skeletal muscle following plantar flexion exercise with high spatial resolution. This approach was extended to in-vivo mapping of free Cr in myocardial disorders.[20] B_0 field inhomogeneity can bias CEST contrast measurements.[21] To obtain B_0-corrected MTR_{asym} (the difference between magnetization transfer ratio values at the positive offsets and the corresponding negative offsets with respect to water), a partial or full z-spectrum is often acquired.[17,22] In the context of post-exercise recovery, computing MTR_{asym} at a single time point using multiple frequency offsets is inadvertently influenced by a time-varying CEST signal from multiple time-points as Cr concentration declines exponentially immediately after exercise. A recent report by Phillip Zhe Sun[23] recently introduced an expedient B_0 inhomogeneity correction algorithm for fast pH imaging that samples only two frequency offsets by exploiting the observation that MTR_{asym} can be modeled as a second-order polynomial function of B_0 inhomogeneity.

Building on these findings, we have developed oxidative phosphorylation CEST (OXCEST) technique, which integrates the fast B_0-correction method[23] to the existing CEST approach to map Cr recovery following exercise in muscle, as previously described.[17-19] Specifically, OXCEST images were acquired at only two frequency offsets: +1.8 and -1.8 ppm. Fast-B_0 correction paradigm was then applied to evaluate pre- and post-exercise MTR_{asym}. We observed that Cr recovered mono-exponentially post-exercise, consistent with the 31P-MRS-derived mono-exponential recovery kinetics of PCr.

2 | THEORY

2.1 | Cr mapping in skeletal muscle

A typical z-spectrum is primarily influenced by the following CEST pools: (i) direct water proton saturation (DS), the largest water signal intensity drop occurring at 0 ppm, (ii) conventional semi-solid magnetization transfer (MT) arising from the "bound" pool of water molecules cross-relaxing with protons in the free water pool, (iii) amide proton transfer (APT) at 3.5ppm, arising from the exchangeable amide protons in the backbone of mobile proteins and peptides, (iv) exchange-relayed nuclear Overhauser effect (rNOE) at -3.5ppm, from aliphatic protons of mobile macromolecules, and (v) Cr CEST at 1.8ppm, from the exchangeable amine protons of Cr.

The asymmetry analysis of the z-spectrum (defined by Equation 1, also called magnetization transfer ratio asymmetry, MTR_{asym}) can separate the symmetrical contribution of DS and MT.

$$\mathrm{MTR_{asym}} = \frac{\mathrm{S(-1.8)-S(+1.8)}}{\mathrm{S(-1.8)}} * 100 \quad (1)$$

At high B_1 (~3 μT) used in this study, the contribution of PCr at ±1.8 ppm is negligible in skeletal muscle, and while APT and rNOE contributions at this offset are negligible in the brain at similar B_1 levels, no such studies exist for skeletal muscle.[24-28] Therefore, without considering B_0 inhomogeneity effects, RF irradiation at only two frequency offsets (±1.8 ppm) is sufficient to quantify the pre-exercise CEST contribution of Cr using MTR_{asym} ($MTR_{asymPre}$). However, as the resonance frequency in MRI is proportional to B_0, even a minor magnetic field inhomogeneity (ΔB_0) can cause substantial frequency shifts in z-spectrum.[21] To correct for this B_0 inhomogeneity, additional frequency offsets are acquired.[17,22]

Following interventions such as mild plantar flexion exercise, intramuscular pH in skeletal muscle remains relatively constant at pressures below 60% of maximal voluntary contraction (MVC) during plantar flexion,[29] and therefore does not significantly influence the CEST contrast. Consequently, exercise-induced change in Cr level, mediated by the CK reaction, is expected to

be the primary contributor to the post-exercise MTR_{asym} ($MTR_{asymPost}$). Additional contribution to $MTR_{asymPost}$ arises from exercise-induced motion, which perturbs B_0,[30] and causes post-exercise ΔB_0 (ΔB_{0Post}) to differ from the pre-exercise ΔB_0 (ΔB_{0Pre}). Given that PCr resynthesis is stoichiometrically coupled with a decrease in free Cr, a higher temporal resolution scan will enable capturing rapid changes in Cr levels. Here, we propose limiting the CEST acquisition to +1.8 and -1.8 ppm, thereby attaining a temporal resolution of 10s (5s per offset x 2 offsets).

2.2 | Fast B_0 correction in OXCEST

To account for B_0 inhomogeneities, we modeled the relationship between $MTR_{asymPre}$ and the corresponding ΔB_{0Pre} across all pixels within a muscle. A second-order polynomial function was fit using least-squares regression to obtain the three coefficients (c_0, c_1, c_2):[23]

$$MTRasymPre(i) = c_0 + c_1 * \Delta B_{0Pre}(i) + c_2 * [\Delta B_{0Pre}(i)]^2 \quad (2)$$

for $i = 1, 2, \ldots, N_{muscle}$.

Function f with fitted coefficients (c_0, c_1, c_2) capture how much the $MTR_{asymPre}$ varies as a function of ΔB_{0Pre} in a given muscle. This fitted function f is then applied to the ΔB_{0Post} values to estimate the portion of the post-exercise MTR_{asym} ($MTR_{asymPost}$) signal that is attributable solely to exercise-induced changes in B_0 alone (i.e. not due to actual physiological change in Cr level):

$$MTR_{asym\Delta B0}(i) = c_0 + c_1 * \Delta B_{0Post}(i) + c_2 * [\Delta B_{0Post}(i)]^2 \quad (3)$$

We hypothesize that the observed MTRasymPost at each pixel results from two additive effects:

1. A B_0-induced change: $MTR_{asym\Delta B0}$
2. A physiologic change due to change in Cr concentration: $MTR_{asym\Delta Cr}$

Thus, the measured $MTR_{asymPost}$ is expressed as:

$$MTR_{asymPost}(i) = MTR_{asym\Delta B0}(i) + MTR_{asym\Delta Cr}(i) \quad (4)$$

By subtracting the estimated B_0-induced component, we isolate the signal due to Cr recovery:

$$MTR_{asym\Delta Cr}(i) = MTR_{asymPost}(i) - MTR_{asym\Delta B0}(i) \quad (5)$$

Next, for an entire muscle, $MTR_{asym\Delta Cr}$ can be calculated as the average of $MTR_{asym\Delta Cr}$ over all the pixels in the muscle.

3 | METHODS

3.1 | Study Design

The protocol was approved by the Institutional Review Board, with informed written consent obtained prior to the scan. Seven healthy adult participants (male: 5, mean age: 34.6 ± 6.1 years) were scanned. Each participant underwent one MR session for OXCEST and another for 31P-MRS, conducted in two separate sessions on different days on a 3T whole-body MR scanner (MAGNETOM Prisma, Siemens Healthcare, Erlangen, Germany). During each acquisition, participants performed mild plantar flexion exercise for 2 minutes at a constant rate of 45 flexions per minute inside the scanner, using an MR-compatible ergometer (Trispect, Ergospect GmbH, Innsbruck, Austria). The pedal pressure was set to 8 PSI, corresponding to 30–40% of each participant's MVC, determined prior to scanning as the peak pressure they could tolerate. The MRI protocols for OXCEST and 31P-MRS are summarized in **Figure S1**.

3.2 | OXCEST MRI

OXCEST data were acquired with a Tx/Rx 1/15-channel 1H knee coil (Siemens Healthcare, Erlangen, Germany). A localizer was first acquired on the right calf of each participant to center the imaging slice on the thickest section of the calf muscle. Before exercise, one image without selective saturation, a B_1 map using a double angle method (30° and 60°),[31] a B_0 map using standard water-saturation shift-referencing (WASSR),[21] and four baseline CEST images[19] were acquired. Immediately following a 2-minute exercise, OXCEST was performed which included post-exercise CEST acquisitions (60 images at 10s temporal resolution), B_0 map, B_1 map, and one reference image without selective saturation. Post-exercise muscle boundaries were delineated from post-exercise CEST images. Acquisition parameters can be found in Chakraborty et al.[32] Briefly, OXCEST imaging parameters were set as follows: TR/TE = 4.7/2.3 ms, slice thickness = 10 mm, flip angle = 10°, B_{1rms} = 3 μT, in-plane resolution = 1.25×1.25 mm^2, matrix size = 128×128, field of view= 160×160 mm^2. OXCEST images were acquired with saturation frequency offsets of ±1.8 ppm relative to the water resonance, achieving a temporal resolution of 10s (5s per offset × 2 offsets). Two dummy scans were included to achieve T1 steady state. For four subjects, the shimming voxel was constrained to a volume encompassing the three muscles of interest. Although MTR_{asym} is relatively stable around optimal RF power level,[33] both pre- and post-exercise OXCEST images were corrected for minor B_1 shifts using an inverse scaling model, assuming a linear relationship between B_1 amplitude and CEST signal intensity.[31]

3.3 | 31P-MRS

31P-MRS was performed with a 1H/31P dual-tuned flex transmit/receive surface coil of 11cm diameter (RAPID Biomedical GmbH, Würzburg-Rimpar, Germany) using an unlocalized free induction decay (FID) sequence: measurements = 96, averages = 2, bandwidth = 5000Hz, and

TR = 5s. The total data acquisition time was 15 minutes: 5 mins of baseline, 2 mins of exercise and 8 mins of post-exercise recovery. The temporal resolution of 31P-MRS was kept at 10s to match the temporal resolution of OXCEST acquisitions.

3.4 | Data analysis

All images and data/statistical analyses were performed on MATLAB v2023b.

3.4.1 | OXCEST

The lateral gastrocnemius (LG), medial gastrocnemius (MG) and soleus (Sol) muscles were manually segmented on the pre-exercise reference image and the post-exercise CEST images. Since exercise can induce shifts in muscle position and subtle geometric changes, including transient hypertrophy during recovery, regions of interest (ROIs) were re-segmented on each post-exercise image until no further changes in muscle boundaries were observed across consecutive time points (usually after 2 minutes). This approach ensured accurate tracking of muscle-specific recovery dynamics. Additionally, anterior tibialis (AT) was also manually segmented. The B_0-corrected $MTR_{asym\Delta Cr}$ signals, reflecting exercise-induced changes in Cr within the three muscles, were calculated as described in section 2.2. The Cr recovery time-constant (T_{Cr}) for each muscle was estimated by fitting a mono-exponential decay model, given by:

$$\mathrm{MTR_{asym\Delta Cr}}\,(\mathrm{t}) = \mathrm{a_0} + \mathrm{a_1} * \mathrm{e}^{\left(-\frac{\mathrm{t}}{\mathrm{T_{Cr}}}\right)} \tag{6}$$

where, a_0 is the baseline value, and a_1 is the amplitude of exponential decay. Initial values were $\mathrm{a_0} = \min\left(MTR_{asym\Delta Cr}\right)$, $\mathrm{a_1} = \max\left(MTR_{asym\Delta Cr}\right) - \min\left(MTR_{asym\Delta Cr}\right)$, and $\mathrm{T_{Cr}} = 60s$. Bound constraints were $\mathrm{a_1} > 0$ and $\mathrm{T_{Cr}} > 0$. Additionally, the pre-exercise B_0-corrected MTR_{asym} value for each muscle was calculated from the coefficient c_0 measured in Equation 2. The exercise-induced increase in MTRasym value was calculated from the coefficient $\mathrm{a_1}$.

To assess B_0-correction effects, the measured MTR_{asym} (Equation 1) was averaged without B_0 correction across all pixels in each muscle at each time point. The mean exercise-induced increase was also computed as the difference between the $MTR_{asymPost}$ at the first time point immediately after exercise and $MTR_{asymPre}$.

3.4.2 | 31P-MRS

The 31P-MRS spectra were phased, baseline-corrected, and fitted with Lorentzians. The PCr peak area was quantified from each FID and normalized to the pre-exercise value. Post-exercise

PCr level was expressed as a percentage of the pre-exercise level. The PCr recovery time-constant, T_{PCr}, was estimated by fitting the data to a mono-exponential growth function:[34]

$$\mathrm{PCr(t)} = \mathrm{b_0} + \mathrm{b_1} * \left(1 - \mathrm{e}^{\left(-\frac{\mathrm{t}}{\mathrm{T_{PCr}}}\right)}\right) \tag{7}$$

where, b_0 is the normalized PCr level at the first post-exercise time point, and b_1 represents the amplitude of recovery.

Additionally, the exercise-induced pH shift was estimated from the chemical shift difference between PCr and inorganic phosphate (P_i) (δ) in 31P-MRS spectra using the adjusted Henderson-Hasselbach equation:[35]

$$pH = pK_A + \log\left(\frac{\delta - \delta_{HA}}{\delta_A - \delta}\right) \tag{8}$$

where $pK_A = 6.75$ is the dissociation constant of P_i, $\delta_{HA} = 3.27$ is the chemical shift of the protonated form of P_i, and $\delta_A = 5.63$ is the chemical shift of the non-protonated form of Pi.

3.5 | Statistical Analysis

Linear regression was performed to evaluate the relationship between T_{Cr} and T_{PCr}. and a two-sided p-value was calculated to test the significance of the association. Lin's concordance correlation coefficient (CCC) was also used to assess the agreement between the two measures. Since the majority of the 31P-MRS signal acquired using a surface coil originates from the gastrocnemius muscle,[18] the mean T_{Cr} values from the LG and MG were used for statistical comparison with T_{PCr}. The coefficient of determination (R^2) and an F-statistic was calculated from the least squares fit of a second-order polynomial relating $MTR_{asymPre}$ to ΔB_{0Pre} in LG, MG, and Sol. 95% confidence intervals (CIs) were calculated for the predicted B_0-corrected $MTR_{asymPre}$ and the exercise-induced increases in MTR_{asym}. Following mono-exponential fitting of Cr recovery in LG, MG and Sol, the root mean squared error (RMSE), R^2, and standard deviation (SD) of residual noise (reported as a percentage of exercise-induced MTR_{asym} increase) were determined. A $P < 0.05$ was considered statistically significant.

4 | RESULTS

4.1 | Demonstration of fast B_0 correction in OXCEST

The proposed OXCEST approach is illustrated in an axial calf muscle section of representative 35-year-old female subject in **Figure 1**. First, the LG, MG, and Sol muscles were manually segmented on a reference anatomical image of the calf (Figure 1A). Pixel-wise $MTR_{asymPre}$ values

were then calculated in the three muscles from OXCEST images (Figure 1B). The corresponding ΔB_{0Pre} map was derived from the pre-exercise WASSR scan (Figure 1C). Figure 1D displays a scatter plot of $MTR_{asymPre}$ versus ΔB_{0Pre} in the MG muscle (orange crosses), along with the second-order polynomial fit (dotted black line) described by the following equation: $MTR_{asymPre} = 5.91 + 152 \times \Delta B_{0Pre} - 191 \times \Delta B_{0Pre}^2$ ($R^2 = 0.97$, $P < 0.001$). The B_0-corrected baseline $MTR_{asymPre}$ value in MG was estimated by setting the corresponding ΔB_{0Pre} to 0 in the previous equation. This yielded a net value of 5.91% (95% CI: 5.74-6.08%) for MG. Similar net $MTR_{asymPre}$ estimation was performed for LG (Figure S2A) and Sol (Figure S2B). The B_0-corrected baseline $MTR_{asymPre}$ values were 6.76 (95% CI: 6.37-7.15%) and 7.2% (95% CI: 7.01-7.29%) for LG and Sol, respectively. Following exercise, the muscles ROIs were re-segmented on the post-exercise CEST-weighted images to account for any movements during exercise. The segmented LG, MG, and Sol regions at the first post-exercise time point (t = 10s) are shown in Figure 1E. Pixel-wise $MTR_{asymPost}$ values were then calculated from the OXCEST images (Figure 1F). The ΔB_{0Post} map was calculated from a WASSR scan acquired following the post-exercise OXCEST scan (Figure 1G). Figure 1H shows a scatterplot of MG $MTR_{asymPost}$ values plotted against ΔB_{0Post} (hollow circles). The black crosses represent $MTR_{asym\Delta B0}$ values predicted using Equation 3. The vertical distance between each $MTR_{asymPost}$ and its associated $MTR_{asym\Delta B0}$ represents the Cr-specific signal change ($MTR_{asym\Delta Cr}$) per pixel. Similar to MG, the $MTR_{asymPost}$ was plotted against ΔB_{0Post} for LG and Sol showing exercise-related Cr increases (Figures S2A and S2B). Plots of $MTR_{asymPre}$ against B_{0Pre} across all subjects in LG, MG, and Sol are shown in **Figures** S3 A-C. The fitted coefficients (c_0, c_1, c_2) are presented in **Table S1**.

4.2 | Post-exercise Cr recovery mapped by OXCEST

The B_0-uncorrected $MTR_{asymPost}$ maps and B_0-corrected $MTR_{asym\Delta Cr}$ maps for the same subject, acquired using OXCEST over a 10-minute post-exercise recovery period, are presented in **Figure 2**. At each time point, pixel intensity reflects the Cr-specific MTR_{asym} signal, with red indicating elevated values and blue indicating values approaching baseline. At 10s post-exercise, all three muscle regions display a marked increase in free Cr concentration. Over the first minute of recovery, Cr concentration rapidly decreases as it rephosphorylates to PCr via the CK reaction.

Table 1 contains estimated values for muscle-wise B_0-corrrected $MTR_{asymPre}$, exercise-induced increases in MTR_{asym}, and R^2 values of function f. The R^2 values for the function f were found to be consistently greater than 0.8 for LG, MG, and Sol (LG: 0.87 ± 0.07, $P < 0.001$; MG: 0.98 ± 0.01, $P < 0.001$; Sol: 0.96 ± 0.03, $P < 0.001$). The B_0-corrrected net $MTR_{asymPre}$ values were found to be 6.03 ± 1.7% in LG, 6.76 ± 0.5% in MG, and 6.87 ± 0.4% in Sol for all the subjects. The 95%

CIs for the estimated B_0-corrrected $MTR_{asymPre}$ were consistently narrow in MG and Sol, as well as in LG of four subjects where constrained shimming was performed. In the remaining three subjects where shimming was not constrained, the absolute B_0 inhomogeneity exceeded 0.1 ppm in the LG only, resulting in broader 95% CIs. In the absence of registering pre- and post-exercise ROIs, the distribution of ΔB_0 values in all three muscles are reported in **Table S2**. LG showed the largest exercise-induced increase in MTR_{asym} (11.4 ± 4.5%), followed by MG (8 ± 2.4%) and Sol (4 ± 2%), all with narrow 95% CIs. Parameters related to mono-exponential fitting of Cr recovery in LG, MG, and Sol are reported in **Table S3**. The R^2 values of the Cr recovery mono-exponential fit were > 0.97 in both LG and MG. Net $MTR_{asymPre}$ values in the LG, MG, and Sol muscles, as well as their post-exercise increases with and without B_0 correction, are presented in **Table S4**. Without B_0-correction, $MTR_{asymPre}$ values ranged from -34% to +28.7%. Analysis of post-exercise increases in MTR_{asym} for AT muscles across all subjects, and the associated T_{Cr} are shown in **Table S5**. Both the metrics showed very high inter-subject variance for TA.

4.3 | Comparison of OXCEST-derived Cr and 31P-MRS-derived PCr recovery

Figure 3 shows the comparison between OXCEST-derived post-exercise Cr recovery kinetics and the ground truth post-exercise PCr recovery kinetics in the same subject. Mono-exponential curves were fitted to the corresponding Cr and PCr recovery profiles. The T_{PCr} measured by 31P-MRS was 32s. Using the OXCEST approach, T_{Cr} values were 27s in LG, 25s in MG, and 29s in Sol. Figure 3C illustrates the fitted post-exercise PCr recovery curve alongside the fitted average post-exercise Cr recovery curve from LG and MG, demonstrating strong agreement between OXCEST and 31P-MRS. T_{PCr} and T_{Cr} for all subjects in this study are summarized in **Table 2**. The average T_{PCr} measured was 51 ± 15s. while the T_{Cr} values were 56 ± 19s (LG), 58 ± 29s (MG), and 52 ± 33s (Sol). The combined T_{Cr} of LG and MG showed a significant correlation with T_{PCr} (R^2 = 0.83, P = 0.005) **(Figure 4)**. A CCC value of 0.81 was found between T_{Cr} and T_{PCr}, suggesting good agreement.[36] Representative Sol recovery curves of subjects 5 and 7 with very low T_{Cr} values are in **Figure S4**. Additionally, exercise did not induce any appreciable changes in pH values in six of the seven subjects, while subject 2 exhibited a pH change of 0.7.

5 | DISCUSSION

In this study, we introduced OXCEST, a novel imaging method for mapping skeletal muscle OXPHOS by applying fast B_0 correction approach for accurately estimating post-exercise Cr recovery kinetics. OXCEST approach further demonstrated strong agreement with the gold-standard technique, 31P-MRS.

By sampling only two frequency offsets, OXCEST generates B_0-corrected, Cr-specific MTR_{asym} images, enabling the capture of post-exercise Cr recovery dynamics at very high temporal resolution. This is critical, as literature reports T_{PCr} values ranging from 20-60s in healthy adults,[11,37] implying that approximately 63% of post-exercise PCr recovery occurs within the first T_{PCr} seconds. Using multiple frequency offsets to compute MTR_{asym} at a single time point, particularly during the post-exercise Cr recovery phase, would inadvertently capture exponentially changing Cr concentrations across offsets, potentially confounding the interpretation of Z-spectra. Given that PCr resynthesis is stoichiometrically coupled with a corresponding decrease in free Cr, capturing the rapid Cr dynamics in muscle demands high temporal resolution. In our study, OXCEST-derived T_{Cr} was significantly correlated with and showed good agreement with 31P-MRS-derived T_{PCr}, a marker of mitochondrial OXPHOS capacity. Additionally, the high R^2 values for the mono-exponential fits in both LG and MG indicate that the model explains over 97% of the variance in the Cr recovery data, supporting the appropriateness of the mono-exponential model for describing post-exercise Cr dynamics. Therefore, OXCEST approach serves as a valuable complement to 31P-MRS technique and offers a non-invasive tool for quantifying skeletal-muscle energetics in clinical settings.

We found that the second-order polynomial relationship between $MTR_{asymPre}$ and ΔB_{0Pre} closely matched previously reported findings in a pH imaging study in rats.[23] In our study, this fit yielded strong R^2 values within the observed ΔB_{0Pre} range of -0.25 to +0.25 ppm, indicating robustness across modest B_0 inhomogeneity. We postulate that the proposed B_0-correction approach in this study will be valid as long as the pre- and post-exercise B_0 are within moderate drifts (0.25 ppm) away from label frequency of 1.8 ppm. Under these conditions, MTR_{asym} can still be reliably estimated using the proposed theory. However, in the absence of shim, large ΔB_0 values may lead to DS-affected CEST signal, compromising the validity of the relationship. Although the second-order polynomial fit adequately modeled the relationship between $MTR_{asymPre}$ and B_{0Pre} across all muscles in the three subjects, higher-order fits may need to be explored where a second order model proves insufficient, possibly due to very narrow Cr peak.

We found the net $MTR_{asymPre}$ values for each muscle group to be approximately 6-7%. Reliable estimation of this parameter depends on the presence of some regions within the muscle where ΔB_0 values are close to zero. If ΔB_0 values in a muscle are confined to a narrow range far from 0 ppm, the estimate of the y-intercept c_0 in Equation 2 will have high variability, resulting in wide 95% CIs. We found that MG and Sol consistently met this criterion, having a fraction of their total ROI with ΔB_0 values close to 0 ppm in all seven subjects. In contrast, the three LG cases

that did not meet this criterion were those in which global shimming was performed instead of localized shimming. CrCEST studies in the literature have reported similar $MTR_{asymPre}$ values,[18-20,27,32,38] supporting the validity of our OXCEST-based quantification. The exercise-induced increase in $MTR_{asym\Delta Cr}$ was found to be highest in LG, followed by MG and Sol, consistent with previous findings.[18,19,27,32,38] The consistently narrow 95% CIs for these measurements further indicate that OXCEST provides robust $MTR_{asymPost}$ maps and that initial shimming was not a limiting factor. Although the exercise-induced increase in $MTR_{asym\Delta Cr}$ differed markedly among muscles, the mean T_{Cr} remained similar across subjects. This is not contradictory because the two parameters probe separate phases of muscle bioenergetics. ΔMTR_{asym} reflects immediate activation by capturing the extent of phosphocreatine depletion and creatine accumulation during the exercise bout. The magnitudes of the increase are consistent with their relative recruitment during plantar flexion at a given workload. In contrast, T_{Cr} represents post-exercise recovery, governed primarily by mitochondrial capacity to resynthesize PCr (and concomitantly rephosphorylate Cr) independent of the magnitude of the preceding depletion. Thus, ΔMTR_{asym} and T_{Cr} offer complementary information, activation versus recovery, highlighting the complexity of muscle bioenergetics rather than a methodological inconsistency. Substantial inter-subject and inter-muscle variability in both activation and recovery further emphasizes the need to interpret group means with caution. Given its relatively low involvement during the exercise protocol,[32] Sol in some subjects exhibited T_{Cr} values that differed substantially from those of the LG and MG. Although the AT muscle is generally considered negative control in plantar flexion exercises, both T_{Cr} values and post-exercise increases in MTR_{asym} in our cohort showed high inter-subject variability. While one study reported less than 1% increase in AT MTR_{asym} following mild exercise,[19] other studies, including unpublished data from our group, have demonstrated measurable AT activation during plantar flexion.[32,39]

The first minute post-exercise is particularly critical for accurately capturing the mono-exponential Cr dynamics. In healthy skeletal muscle, T_{PCr} ranges between 20-60s.[11,37] Given the exponential nature of PCr recovery, a muscle with T_{PCr} = 20 s recovers ~95% of PCr by 1 minute post-exercise, whereas a muscle with T_{PCr} = 60 s recovers ~63% by the same time. This highlights the advantage of OXCEST's expedient B_0 correction algorithm, which supports 10s temporal resolution, allowing detailed sampling of the steep early recovery phase. The strong correlation between OXCEST-derived T_{Cr} and 31P-MRS-derived T_{PCr} supports the accuracy of this method.

In one study involving strenuous exercise,[40] elevated T_2 relaxation times were inversely correlated with T_{PCr}. Since PCr, and Cr are stoichiometrically coupled, any factor affecting PCr kinetics is

expected to influence Cr kinetics as well. In the absence of full z-spectra, it is difficult to assess the extent of overlap between T_2-influenced direct water saturation and the Cr pool at +1.8 ppm. A previous study has shown that T_2 did not change appreciably after mild exercise.[19] While participants in our study also performed mild exercise, we did not investigate the potential effects of T_2* on MTR_{asym}.

Acquiring pre-exercise MTR_{sym} values remain important for several reasons, as is also standard practice in conventional CrCEST and 31P-MRS protocols. First, in individuals with neuromuscular disorders who may be unable to complete exercise or remain still during the post-exercise phase, a pre-exercise baseline serves as a critical reference and aids in Cr mapping. Second, lactate accumulation can lead to persistent changes in pH, which may not return to baseline quickly and can further complicate interpretation of recovery dynamics. This is why we recommend using the pre-exercise MTR_{asym} values to estimate the fitting coefficients (c_0, c_1, c_2) in OXCEST.

This study has certain limitations. We used WASSR approach to generate ΔB_0 maps pre- and post-exercise.[21] A foundational assumption of the OXCEST framework is that the B_0 inhomogeneity remains stable post-exercise. However, gradual B_0 field drift may still occur due to heating of scanner components during gradient-intensive MR sequences, a phenomenon observed in NOE experiments.[24,41] Similar local magnetic field drifts are a well-recognized issue in functional MRI studies.[42] Additionally, post-exercise changes such as muscle recovery or subtle calf movement can affect the B_0, introducing errors in correction. To mitigate such effects, an interleaved gradient echo-based B_0 mapping sequence could be implemented alongside the CEST acquisition to regress out the effect of such frequency drifts.[43] Acquiring dynamic ΔB_{0Post} for each frequency offset pairs would enable accurate computation of $MTR_{asym\Delta B0}$ (Equation 3), and subsequently $MTR_{asym\Delta Cr}$ and T_{Cr}, making OXCEST more robust to motion and the resulting B_0 fluctuations over time. Secondly, our manuscript included data from healthy volunteers only. In subjects with neuromuscular diseases, the lactate accumulation can significantly change the pH, which will change the exchange rates, resulting in underestimation of the CEST contrast.[20] Notably, pH-specific changes have been accounted for in a recent report by Philip Zhe Sun through the inclusion of an additive correction term.[23] Finally, OXCEST and 31P-MRS recovery data were acquired during two separate sessions conducted on different days. Although care was taken to ensure that exercise bouts were consistent across sessions, inter-session variability may still influence direct comparisons. A large-scale study with simultaneous monitoring of PCr and Cr recovery kinetics is needed to confirm the reproducibility and robustness of these findings.

6 | CONCLUSION

In this study, we introduced OXCEST, an advanced technique for mapping skeletal muscle OXPHOS by quantifying CEST effects of Cr using acquisitions at two frequency offsets. We demonstrated its utility by mapping dynamic changes in skeletal muscle metabolism post-exercise in healthy participants and comparing the results with the gold standard 31P-MRS technique. This validation highlights OXCEST's potential for clinical translation as a potential non-invasive alternative for assessing in vivo muscle mitochondrial OXPHOS. Furthermore, the underlying principles of OXCEST are broadly applicable and adapted to other CEST-based imaging applications, particularly those requiring high temporal resolution following a physiological or pharmacological intervention.

ACKNOWLEDGEMENTS

The authors thank Ms. Jennifer Valley and Dr. Mitchell Taylor for their technical support and Ms. Pamela Adede for her assistance with participant recruitment.

DATA AVAILABILITY STATEMENT

Data will be made available upon request.

TABLES

Table 1: Metrics derived from OXCEST method

ID	$MTR_{asymPre}$ versus $B0_{Pre}$ (R^2)			B_0-corrected $MTR_{asymPre}$			Exercise-induced increase in MTR_{asym}		
	LG	MG	Sol	LG	MG	Sol	LG	MG	Sol
1	0.833	0.98	0.912	4.49 (3.1,5.9)	7.1 (7,7.2)	6.9 (6.8,7.1)	18.3 (17.6, 19)	8.9 (8.7, 9.2)	6 (5.8, 6.2)
2	0.962	0.992	0.967	6.8 (6.4 ,7.2)	5.9 (5.7,6.1)	7.2 (7,7.3)	9.3 (9.1 ,9.5)	9.3 (9.1 ,9.5)	2.4 (2.1,2.6)
3	0.74	0.982	0.955	5.7 (5.4 ,5.9)	6.3 (5.6,6.9)	7.1 (7 ,7.2)	6.4 (6,6.8)	5.9 (5.7,6.1)	1.6 (1.1 ,2)
4	0.841	0.975	0.927	8 (5,10.9)	7.4 (7.2,7.5)	6.8 (6.7 ,6.9)	10.6 (10.4,10.8)	12.1 (11.9,12.3)	5.3 (5.1,5.5)
5	0.881	0.981	0.982	8.7 (5.5,11.8)	6.8 (6.6,6.9)	7 (6.9,7.2)	5.3 (5.1,5.5)	4.1 (3.9,4.3)	1.5 (1.4,1.7)
6	0.952	0.996	0.993	4.5 (-3.8,12.7)	6.4 (6.3,6.6)	5.9 (5.8,6)	15.8 (15.5,16.2)	7.8 (7.7,8)	6.3 (6.1,6.5)
7	0.86	0.985	0.981	4 (0.5,7.4)	7.4 (7.3,7.5)	7.2 (7.1,7.4)	14.1 (13.6,14.6)	8.2 (7.9,8.5)	5 (4.9,5.2)
Mean	0.87	0.98	0.96	6.03	6.76	6.87	11.40	8.04	4.01
SD	0.07	0.01	0.03	1.71	0.54	0.42	4.50	2.36	1.95

Some values are reported as mean (95% confidence interval).

Table 2: Recovery time constants derived from OXCEST and 31P-MRS (n = 7)

ID	31P-MRS T_{PCr}(s)	OXCEST T_{Cr}(s)		
		LG	MG	Sol
1	41.06	46.15	66.54	90.4
2	32.24	27.19	25.27	29.33
3	50.43	71.04	65.23	72.46
4	42.74	38.94	21.37	96.52
5	83.28	87.96	112.39	14.56
6	47.24	65.95	45.34	49.84
7	59.77	56.66	67.92	11.75
Mean	50.97	56.27	57.72	52.12
SD	15.36	19.14	28.67	32.55

Figure Legends

Figure 1. Demonstration of the Oxidative Phosphorylation Chemical Exchange Saturation Transfer (OXCEST) approach in a 35-year-old female participant. (A) Segmentation of the lateral gastrocnemius (LG), medial gastrocnemius (MG), and soleus (Sol) muscles on a pre-exercise axial anatomical calf image. (B-C) Pre-exercise magnetization transfer ratio asymmetry ($MTR_{asymPre}$) map acquired at +1.8 ppm and the corresponding B_0 inhomogeneity (ΔB_{0Pre}) map derived from a water-saturation shift-referencing (WASSR) scan, both overlaid on the segmented muscle masks. (D) Pixel-wise regression of $MTR_{asymPre}$ against ΔB_{0Pre} in MG; the dotted line represents the second-order polynomial fit. (E) Segmentation of the three muscles on a post-exercise axial anatomical calf image. (F-G) Post-exercise MTR_{asym} ($MTR_{asymPost}$) and ΔB_0 (ΔB_{0Post}) maps acquired following mild plantar-flexion exercise. (H) Scatterplot of $MTR_{asymPost}$ versus ΔB_{0Post} in MG (circles). Black crosses indicate the expected value of MTR_{asym} due solely to B_0 changes ($\mathrm{MTR}_{\mathrm{asym}\Delta \mathrm{B0}}$), assuming no change in creatine (Cr) concentration. Thus, the Cr-related change in MTR_{asym} is quantified as the vertical distance between each circle and its corresponding cross, representing the ΔB_0-corrected Cr effect.

Figure 2. Effect of Oxidative Phosphorylation Chemical Exchange Saturation Transfer (OXCEST)-based B_0 correction on post-exercise MTR_{asym}, acquired with a temporal resolution of 10s over a 10-minute post-exercise recovery period. Each frame displays pixel-wise post-exercise magnetization transfer ratio asymmetry ($MTR_{asymPost}$) (in %) in a representative axial slice of the lower leg encompassing the soleus (Sol), lateral gastrocnemius (LG), and medial gastrocnemius (MG) muscles: (A) without B_0 correction, and (B) after B_0 correction. Without correction, MTR_{asym} values often fell outside the physiologically reasonable range (e.g. negative or abnormally large values). After correction, elevated MTR_{asym} immediately after exercise (red pixels, 10-60s after exercise) reflects an increased free creatine concentration, which decays exponentially over time. This spatiotemporally resolved mapping of Cr dynamics highlights muscle-specific variations in mitochondrial OXPHOS capacity.

Figure 3. Comparison of post-exercise phosphocreatine (PCr) and creatine (Cr) recovery kinetics measured using 31P-Magnetic Resonance Spectroscopy (31P-MRS) and Oxidative Phosphorylation Chemical Exchange Saturation Transfer (OXCEST), respectively, in a representative subject. (A) Non-localized 31P-MRS-derived PCr signal demonstrates mono-exponential post-exercise growth. (B) OXCEST-derived Cr signal exhibits mono-exponential decay in all three muscles: lateral gastrocnemius (LG), medial gastrocnemius (MG), and soleus (Sol). (C) Mono-exponential curves are fitted to the PCr recovery and to the mean Cr recovery of

LG and MG. The PCr recovery time constant derived from 31P-MRS (T_{PCr} = 32s) closely matched the mean Cr recovery time constant (T_{Cr} = 26s) from OXCEST. The faster B_0 correction in OXCEST enables higher temporal resolution, allowing for detailed capture of early post-exercise dynamics and improved accuracy of kinetic modeling.

Figure 4. Regression analysis comparing creatine (Cr) recovery time constant (T_{Cr}) measured using Oxidative Phosphorylation Chemical Exchange Saturation Transfer (OXCEST) with phosphocreatine (PCr) recovery time constant (T_{PCr}) determined using 31P-Magnetic Resonance Spectroscopy (31P-MRS). A significant linear correlation was observed between T_{Cr} and T_{PCr} (R^2 = 0.83, P = 0.005), indicating strong agreement between the two measurements. Dashed ellipse represents the 95% confidence region.

References

1. Pesta D, Anadol-Schmitz E, Sarabhai T, et al. Determinants of increased muscle insulin sensitivity of exercise-trained versus sedentary normal weight and overweight individuals. *Sci Adv.* 2025;11(1):eadr8849.
2. Kawamata H, Manfredi G. Proteinopathies and OXPHOS dysfunction in neurodegenerative diseases. *J Cell Biol.* 2017;216(12):3917-3929.
3. Mancuso M, Angelini C, Bertini E, et al. Fatigue and exercise intolerance in mitochondrial diseases. Literature revision and experience of the Italian Network of mitochondrial diseases. *Neuromuscul Disord.* 2012;22 Suppl 3(3-3):S226-229.
4. Wallace DC. A mitochondrial bioenergetic etiology of disease. *J Clin Invest.* 2013;123(4):1405-1412.
5. Xu Y, Xue D, Bankhead A, 3rd, Neamati N. Why All the Fuss about Oxidative Phosphorylation (OXPHOS)? *J Med Chem.* 2020;63(23):14276-14307.
6. Acin-Perez R, Beninca C, Shabane B, Shirihai OS, Stiles L. Utilization of Human Samples for Assessment of Mitochondrial Bioenergetics: Gold Standards, Limitations, and Future Perspectives. *Life (Basel).* 2021;11(9).
7. Meyerspeer M, Boesch C, Cameron D, et al. (31) P magnetic resonance spectroscopy in skeletal muscle: Experts' consensus recommendations. *NMR Biomed.* 2020;34(5):e4246.
8. Kemp GJ, Ahmad RE, Nicolay K, Prompers JJ. Quantification of skeletal muscle mitochondrial function by 31P magnetic resonance spectroscopy techniques: a quantitative review. *Acta Physiol (Oxf).* 2015;213(1):107-144.
9. Meyer RA. A linear model of muscle respiration explains monoexponential phosphocreatine changes. *Am J Physiol.* 1988;254(4 Pt 1):C548-553.
10. Lanza IR, Bhagra S, Nair KS, Port JD. Measurement of human skeletal muscle oxidative capacity by 31P-MR spectroscopy: a cross-validation with in vitro measurements. *J Magn Reson Imaging.* 2011;34(5):1143-1150.
11. Lewsey SC, Weiss K, Schar M, et al. Exercise intolerance and rapid skeletal muscle energetic decline in human age-associated frailty. *JCI Insight.* 2020;5(20).
12. Hargreaves M, Spriet LL. Skeletal muscle energy metabolism during exercise. *Nat Metab.* 2020;2(9):817-828.
13. Walsh B, Tonkonogi M, Soderlund K, Hultman E, Saks V, Sahlin K. The role of phosphorylcreatine and creatine in the regulation of mitochondrial respiration in human skeletal muscle. *J Physiol.* 2001;537(Pt 3):971-978.
14. Jett S, Boneu C, Zarate C, et al. Systematic review of (31)P-magnetic resonance spectroscopy studies of brain high energy phosphates and membrane phospholipids in aging and Alzheimer's disease. *Front Aging Neurosci.* 2023;15:1183228.
15. Jing Y, Haeger A, Boumezbeur F, Binkofski F, Reetz K, Romanzetti S. Neuroenergetic alterations in neurodegenerative diseases: A systematic review and meta-analysis of in vivo(31)P-MRS studies. *Ageing Res Rev.* 2024;101:102488.
16. Sassani M, Alix JJ, McDermott CJ, et al. Magnetic resonance spectroscopy reveals mitochondrial dysfunction in amyotrophic lateral sclerosis. *Brain.* 2020;143(12):3603-3618.
17. Haris M, Nanga RP, Singh A, et al. Exchange rates of creatine kinase metabolites: feasibility of imaging creatine by chemical exchange saturation transfer MRI. *NMR Biomed.* 2012;25(11):1305-1309.
18. Kogan F, Haris M, Debrosse C, et al. In vivo chemical exchange saturation transfer imaging of creatine (CrCEST) in skeletal muscle at 3T. *J Magn Reson Imaging.* 2014;40(3):596-602.

19. Kogan F, Haris M, Singh A, et al. Method for high-resolution imaging of creatine in vivo using chemical exchange saturation transfer. *Magn Reson Med.* 2014;71(1):164-172.
20. Haris M, Singh A, Cai K, et al. A technique for in vivo mapping of myocardial creatine kinase metabolism. *Nat Med.* 2014;20(2):209-214.
21. Kim M, Gillen J, Landman BA, Zhou J, van Zijl PC. Water saturation shift referencing (WASSR) for chemical exchange saturation transfer (CEST) experiments. *Magn Reson Med.* 2009;61(6):1441-1450.
22. Ju L, Schar M, Wang K, et al. Mitochondrial oxidative phosphorylation capacity in skeletal muscle measured by ultrafast Z-spectroscopy (UFZ) MRI at 3T. *Magn Reson Med.* 2025;93(3):1273-1284.
23. Sun PZ. Fast correction of B(0) field inhomogeneity for pH-specific magnetization transfer and relaxation normalized amide proton transfer imaging of acute ischemic stroke without Z-spectrum. *Magn Reson Med.* 2020;83(5):1688-1697.
24. Jones CK, Huang A, Xu J, et al. Nuclear Overhauser enhancement (NOE) imaging in the human brain at 7T. *Neuroimage.* 2013;77:114-124.
25. van Zijl PCM, Lam WW, Xu J, Knutsson L, Stanisz GJ. Magnetization Transfer Contrast and Chemical Exchange Saturation Transfer MRI. Features and analysis of the field-dependent saturation spectrum. *Neuroimage.* 2018;168:222-241.
26. Jin T, Wang P, Zong X, Kim SG. MR imaging of the amide-proton transfer effect and the pH-insensitive nuclear overhauser effect at 9.4 T. *Magn Reson Med.* 2013;69(3):760-770.
27. DeBrosse C, Nanga RPR, Wilson N, et al. Muscle oxidative phosphorylation quantitation using creatine chemical exchange saturation transfer (CrCEST) MRI in mitochondrial disorders. *JCI Insight.* 2016;1(18):e88207.
28. Chen L, Barker PB, Weiss RG, van Zijl PCM, Xu J. Creatine and phosphocreatine mapping of mouse skeletal muscle by a polynomial and Lorentzian line-shape fitting CEST method. *Magn Reson Med.* 2019;81(1):69-78.
29. Homma T, Hamaoka T, Sako T, et al. Muscle oxidative metabolism accelerates with mild acidosis during incremental intermittent isometric plantar flexion exercise. *Dyn Med.* 2005;4(1):2.
30. Liu J, de Zwart JA, van Gelderen P, Murphy-Boesch J, Duyn JH. Effect of head motion on MRI B(0) field distribution. *Magn Reson Med.* 2018;80(6):2538-2548.
31. Singh A, Cai K, Haris M, Hariharan H, Reddy R. On B1 inhomogeneity correction of in vivo human brain glutamate chemical exchange saturation transfer contrast at 7T. *Magn Reson Med.* 2013;69(3):818-824.
32. Chakraborty K, Burman R, Nisar S, et al. Reliability of In Vivo Creatine-Weighted Chemical Exchange Saturation Transfer (CrCEST) MRI in Calf Skeletal Muscle of Healthy Volunteers at 3 T. *J Magn Reson Imaging.* 2024.
33. Sun PZ, Zhou J, Huang J, van Zijl P. Simplified quantitative description of amide proton transfer (APT) imaging during acute ischemia. *Magn Reson Med.* 2007;57(2):405-410.
34. Forbes SC, Slade JM, Meyer RA. Short-term high-intensity interval training improves phosphocreatine recovery kinetics following moderate-intensity exercise in humans. *Appl Physiol Nutr Metab.* 2008;33(6):1124-1131.
35. Valkovic L, Chmelik M, Krssak M. In-vivo(31)P-MRS of skeletal muscle and liver: A way for non-invasive assessment of their metabolism. *Anal Biochem.* 2017;529:193-215.
36. Clarke CJ, Gurka MJ, Norton PT, Kramer CM, Hoyer AW. Assessment of the accuracy and reproducibility of RV volume measurements by CMR in congenital heart disease. *JACC Cardiovasc Imaging.* 2012;5(1):28-37.
37. Menon RG, Xia D, Katz SD, Regatte RR. Dynamic (31)P-MRI and (31)P-MRS of lower leg muscles in heart failure patients. *Sci Rep.* 2021;11(1):7412.

38. Armbruster RR, Kumar D, Benyard B, et al. Personalized and muscle-specific OXPHOS measurement with integrated CrCEST MRI and proton MR spectroscopy. *Nat Commun.* 2024;15(1):5387.
39. Schur GM, Dunn J, Nguyen S, et al. In vivo assessment of OXPHOS capacity using 3 T CrCEST MRI in Friedreich's ataxia. *J Neurol.* 2022;269(5):2527-2538.
40. Schmid AI, Schewzow K, Fiedler GB, et al. Exercising calf muscle T(2) * changes correlate with pH, PCr recovery and maximum oxidative phosphorylation. *NMR Biomed.* 2014;27(5):553-560.
41. Windschuh J, Zaiss M, Ehses P, Lee JS, Jerschow A, Regatte RR. Assessment of frequency drift on CEST MRI and dynamic correction: application to gagCEST at 7 T. *Magn Reson Med.* 2019;81(1):573-582.
42. Kopel R, Sladky R, Laub P, et al. No time for drifting: Comparing performance and applicability of signal detrending algorithms for real-time fMRI. *Neuroimage.* 2019;191:421-429.
43. Poblador Rodriguez E, Moser P, Dymerska B, et al. A comparison of static and dynamic ΔB(0) mapping methods for correction of CEST MRI in the presence of temporal B(0) field variations. *Magn Reson Med.* 2019;82(2):633-646.

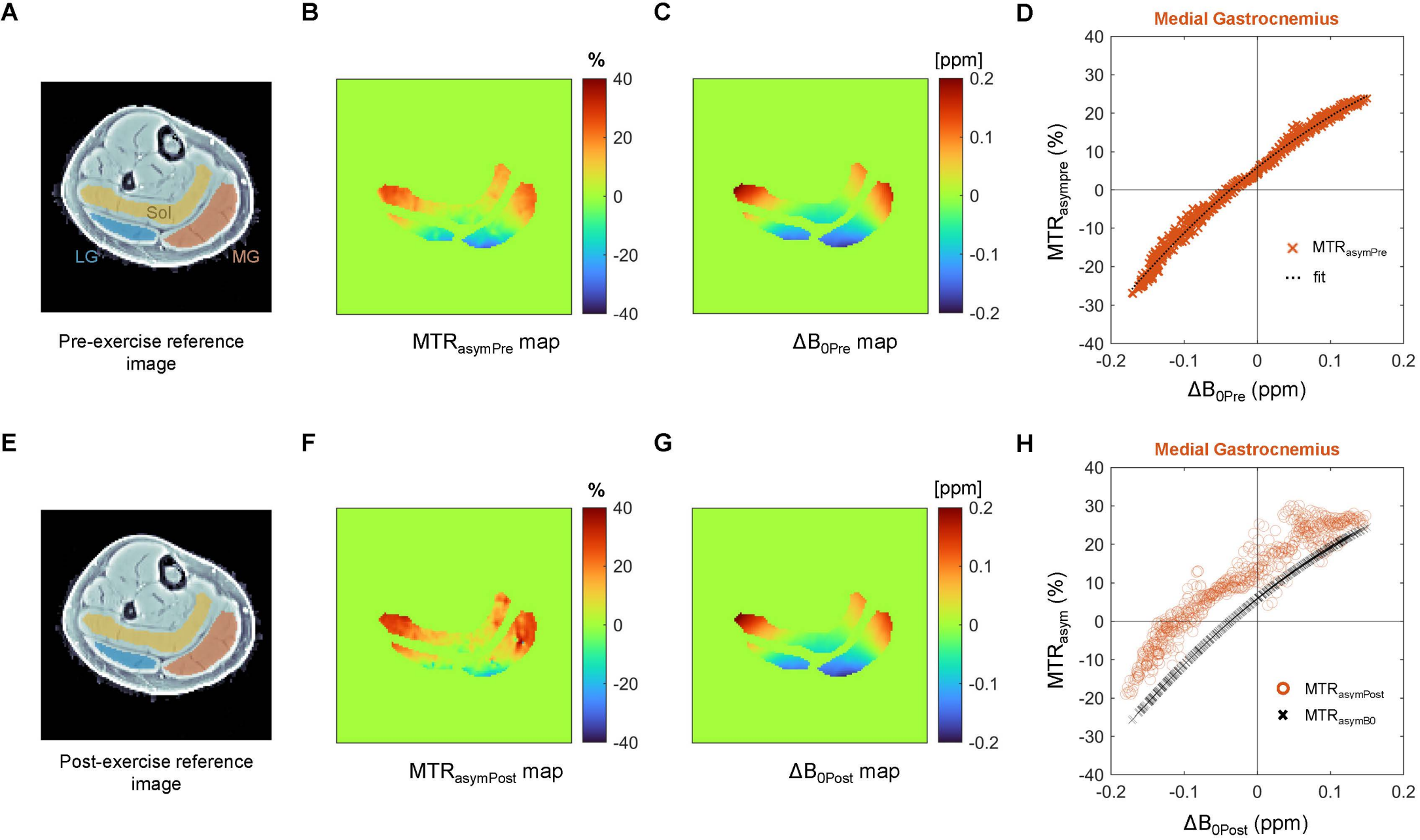
A
Sol
LG
MG
Pre-exercise reference image
B
%
40
20
0
-20
-40
MTR$_{asymPre}$ map
C
[ppm]
0.2
0.1
0
-0.1
-0.2
ΔB$_{0Pre}$ map
D
Medial Gastrocnemius
MTR$_{asympre}$ (%)
ΔB$_{0Pre}$ (ppm)
MTR$_{asymPre}$
fit
E
Post-exercise reference image
F
MTR$_{asymPost}$ map
G
ΔB$_{0Post}$ map
H
Medial Gastrocnemius
MTR$_{asym}$ (%)
ΔB$_{0Post}$ (ppm)
MTR$_{asymPost}$
MTR$_{asymB0}$

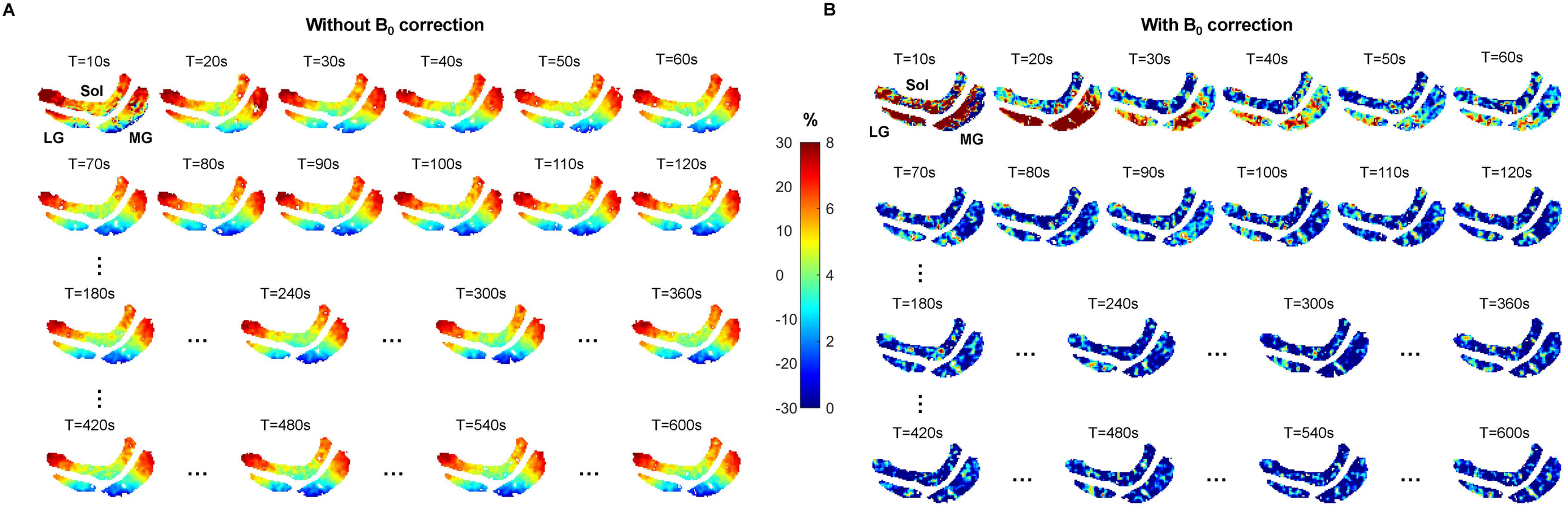
A
Without B_0 correction
T=10s
T=20s
T=30s
T=40s
T=50s
T=60s
Sol
LG
MG
T=70s
T=80s
T=90s
T=100s
T=110s
T=120s
T=180s
T=240s
T=300s
T=360s
T=420s
T=480s
T=540s
T=600s
%
30
20
10
0
-10
-20
-30
8
6
4
2
0
B
With B_0 correction
T=10s
T=20s
T=30s
T=40s
T=50s
T=60s
Sol
LG
MG
T=70s
T=80s
T=90s
T=100s
T=110s
T=120s
T=180s
T=240s
T=300s
T=360s
T=420s
T=480s
T=540s
T=600s

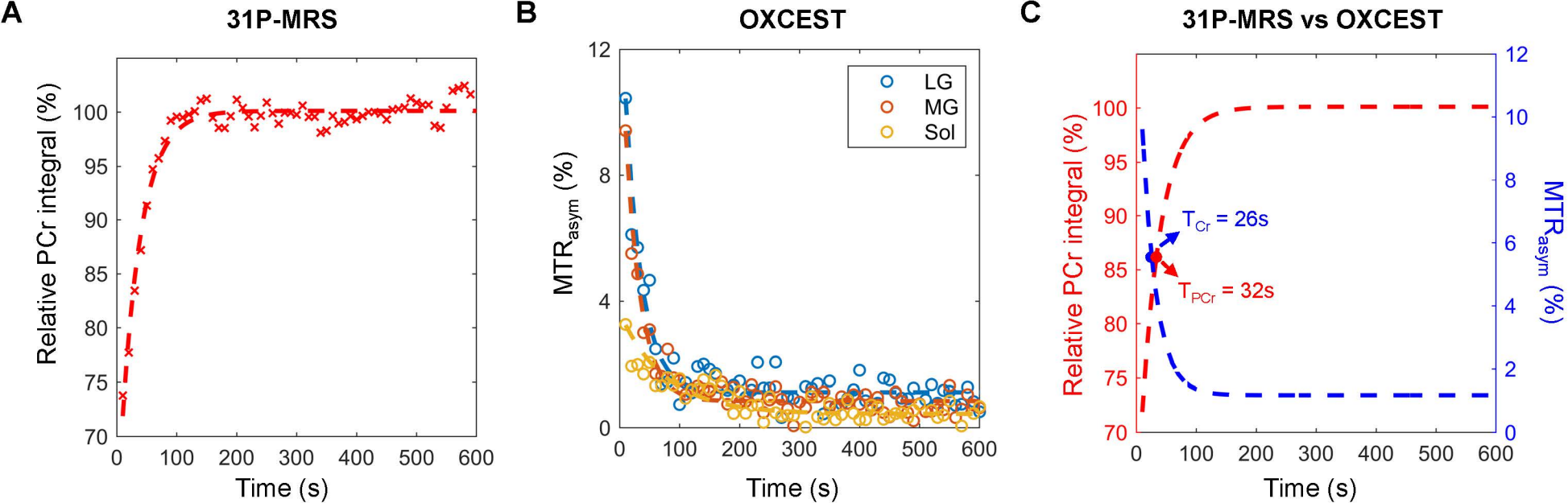
A
31P-MRS
Relative PCr integral (%)
Time (s)
B
OXCEST
LG
MG
Sol
MTRasym (%)
Time (s)
C
31P-MRS vs OXCEST
Relative PCr integral (%)
MTRasym (%)
TCr = 26s
TPCr = 32s
Time (s)

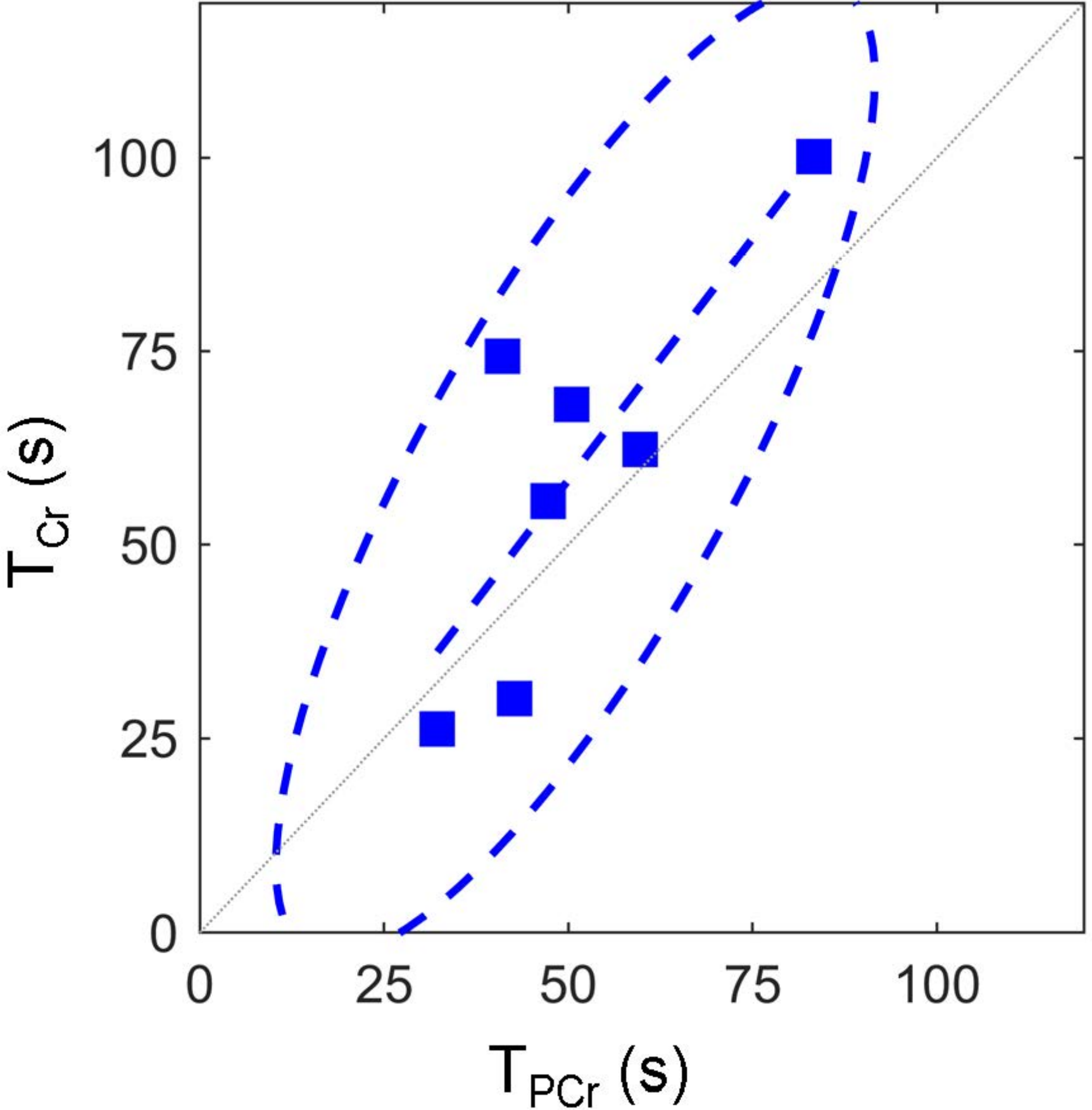
100
75
50
25
0
0
25
50
75
100
T_{Cr} (s)
T_{PCr} (s)